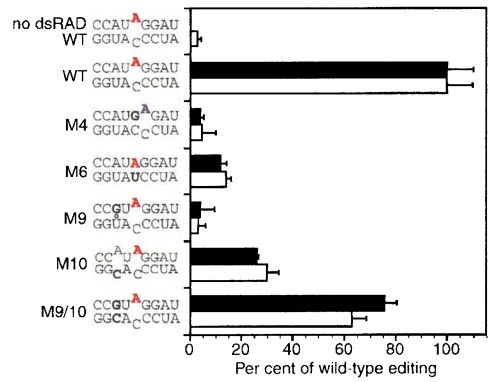

FIG. 3 *In vitro* editing has similar sequence requirements as editing *in vivo*. The graph compares *in vitro* (open bars) and *in vivo* (filled bars) editing for 5 HDV mutants. Bar length reflects per cent editing normalized to wild-type (100%). Antigenomic sequences surrounding the editing site are shown (1,016–1,008 paired with 584–576) with mutated nucleotides (bold), the amber/W site (red) and a potential new editing site created in mutant M4 (blue) indicated. Mutations were restricted to those that did not alter the encoded HDAg amino-acid sequence, and to maintain replication, to those that, in the absence of editing, maintained the stop codon at the amber/W site. Virion production, which is critically dependent on editing, was sharply reduced for all mutants except M9/10 (J.L.C., data not shown). Before normalization, wild-type editing *in vivo* was $25 \pm 3\%$ or $21 \pm 4\%$ as assayed with *STyI* or *DsaI*, respectively, and *in vitro*, $44 \pm 4\%$ (*StyI*) and $46 \pm 3\%$ (*DsaI*).
METHODS. For *in vitro* reactions (20 μl; $n = 4$), 5 fmol antigenomic RNA (1/3Δ 1.2mer) was incubated with dsRAD (7.5 μl) for 2 h. For editing in cells, cDNA constructs that expressed replication-competent HDV RNA were transfected into HuH7 cells, and RNA collected 12 days post-transfection as described[11] ($n = 3$ except for M6 where $n = 2$). RNAs edited *in vitro* or *in vivo* were assayed using *StyI* (wt, M4, M6, M10) or, because some mutations destroyed the *StyI* site, *DsaI* (wt, M9, M9/10).

vitro system described here may represent the first example of an RNA editing reaction to occur *in vitro* with purified components. *Note added in proof*: Another *in vitro* reaction involving purified dsRAD has now been described[27]. □

Received 4 December 1995; accepted 2 February 1996.

1. Wu, J. C. *et al. J. Virol.* **65,** 1099–1104 (1991).
2. Ryu, W. S., Bayer, M. & Taylor, J. *J. Virol.* **66,** 2310–2315 (1992).
3. Rizzetto, M. *Hepatology* **3,** 729–737 (1983).
4. Lai, M. M. C. *A. Rev. Biochem.* **64,** 259–286 (1995).
5. Wang, K. S. *et al. Nature* **323,** 508–514 (1986).
6. Luo, G. X. *et al. J. Virol.* **64,** 1021–1027 (1990).
7. Kuo, M. Y., Chao, M. & Taylor, J. *J. Virol.* **63,** 1945–1950 (1989).
8. Chao, M., Hsieh, S. Y. & Taylor, J. *J. Virol.* **64,** 5066–5069 (1990).
9. Tang, J. R. *et al. J. med. Virol.* **42,** 1–6 (1994).
10. Zheng, H., Fu, T. B., Lazinski, D. & Taylor, J. *J. Virol.* **66,** 4693–4697 (1992).
11. Casey, J. L., Bergmann, K. F., Brown, T. L. & Gerin, J. L. *Proc. natn. Acad. Sci. U.S.A.* **89,** 7149–7153 (1992).
12. Casey, J. L. & Gerin, J. L. *J. Virol.* **69,** 7593–7600 (1995).
13. Bass, B. L. & Weintraub, H. *Cell* **55,** 1089–1098 (1988).
14. Wagner, R. W., Smith, J. E., Cooperman, B. S. & Nishikura, K. *Proc. natn. Acad. Sci. U.S.A.* **86,** 2647–2651 (1989).
15. Polson, A. G. & Bass, B. L. *EMBO J.* **13,** 5701–5711 (1994).
16. Bass, B. L. in *The RNA World* (eds Gesteland, R. & Atkins, J.) 383–418 (Cold Spring Harbor Laboratory Press, New York, 1993).
17. Bass, B. L. & Weintraub, H. *Cell* **48,** 607–613 (1987).
18. Wagner, R. W. & Nishikura, K. *Molec. cell. Biol.* **8,** 770–777 (1988).
19. Netter, H. J. *et al. J. Virol.* **69,** 1687–1692 (1995).
20. Hurst, S. R., Hough, R. F., Aruscavage, P. J. & Bass, B. L. *RNA* **1,** 1051–1060 (1995).
21. Lomeli, H. *et al. Science* **266,** 1709–1713 (1994).
22. Rueter, S. M., Burns, C. M.. Coode, S. A., Mookherjee, P. & Emeson, R. B. *Science* **267,** 1491–1494 (1995).
23. Yang, J.-H., Sklar, P., Axel, R. & Maniatis, T. *Nature* **374,** 77–81 (1995).
24. Melcher, T., Maas, S., Higuchi, M., Keller, W. & Seeburg, P. H. *J. biol. Chem.* **270,** 8566–8570 (1995).
25. Hough, R. F. & Bass, B. L. *J. biol. Chem.* **269,** 9933–9939 (1994).
26. Saccomanno, L. & Bass, B. L. *Molec. cell. Biol.* **14,** 5425–5432 (1994).
27. Melcher, T. *et al. Nature* **379,** 460–464 (1996).

ACKNOWLEDGEMENTS. We thank R. Hough and S. Hurst for providing purified dsRAD and T. Brown for technical assistance. This work was supported by funds to B.L.B. from the NIH, the Pew Scholars Program, and the David and Lucile Packard Foundation, and by funds to J.L.C. from the NIH. B.L.B. is an HHMI assistant investigator.

CORRESPONDENCE and requests for materials should be addressed to B.L.B. (e-mail: bas@tulip.med.utah.edu).

A new pattern for helix–turn–helix recognition revealed by the PU.1 ETS-domain–DNA complex

Ramadurgam Kodandapani*, Frédéric Pio*, Chao-Zhou Ni*, Gennaro Piccialli†, Michael Klemsz‡, Scott McKercher*, Richard A. Maki*§ & Kathryn R. Ely*

* La Jolla Cancer Research Center at The Burnham Institute, 10901 North Torrey Pines Road, La Jolla, California 92037, USA
† Dipartimento di Chimica Organica e Biologica, Universita degli Studi di Napoli Federico II, 80134 Napoli, Italy
§ Neurocrine Biosciences, San Diego, California 92121, USA

THE Ets family of transcription factors, of which there are now about 35 members[1,2], regulate gene expression during growth and development. They share a conserved domain of around 85 amino acids[3] which binds as a monomer to the DNA sequence 5′-C/AGGAA/T-3′. We have determined the crystal structure of an ETS domain complexed with DNA, at 2.3-Å resolution. The domain is similar to α + β (winged) 'helix–turn–helix' proteins and interacts with a ten-base-pair region of duplex DNA which takes up a uniform curve of 8°. The domain contacts the DNA by a novel loop–helix–loop architecture. Four of the amino acids that directly interact with the DNA are highly conserved: two arginines from the recognition helix lying in the major groove, one lysine from the 'wing' that binds upstream of the core GGAA sequence, and another lysine, from the 'turn' of the 'helix–turn–helix' motif, which binds downstream and on the opposite strand.

The PU.1 *[Spi-1, Spfi-1]* transcription factor is an Ets protein expressed in haematopoietic cells[4,5]. PU.1 is a regulatory protein for differentiation of monocytes and macrophages and for B-cell maturation (reviewed in ref. 2). The ETS domain of PU.1 was co-crystallized with a 16 base-pair oligonucleotide containing the recognition sequence[6]. The structure was solved by the multiple isomorphous replacement and anomalous scattering (MIRAS) method (Table 1). The electron density was clearly defined (Fig. 1) for residues 171 to 258, which encompasses the entire conserved ETS domain. The PU.1 domain assumes a tight globular structure ($33 \times 34 \times 38$ Å^3) formed by three α-helices and a four-stranded antiparallel β-sheet (Fig. 1). The domain topology is similar to the structures of other Ets family proteins Fli-1 (ref. 7), murine Ets-1 (ref. 8) and human Ets-1 (ref. 9) determined in solution by NMR. The structural studies revealed a common folding pattern for ETS domains that is similar to α + β helix–turn–helix (HTH) DNA-binding proteins including CAP[10] and resembles 'winged' HTH proteins such as GH5 (ref. 11), HNF-3γ (ref. 12) and HSF (ref. 13). There are three sites of protein–DNA contact: the recognition helix (α3), the loop between β-strands 3 and 4 (a 'wing') and the turn in the HTH motif (α2–turn–α3). The turn between α2 and α3 is longer than the equivalent in many other HTH proteins, and is actually a loop. The DNA-binding motif in PU.1, and probably other members of the Ets family, can be described more appropriately as a loop–helix–loop motif. Therefore the large Ets family defines a new variant subclass of the helix–turn–helix DNA-binding proteins with a novel mode of DNA recognition.

The protein–DNA contacts in the PU.1 complex are detailed in Fig. 2. Four strictly conserved residues on the surface of the domain are likely to be important for DNA binding by all members of the Ets family. Arg 232 and Arg 235 emanate from helix α3 and contact bases in the GGAA sequence in the major groove. These contacts represent the core structure for DNA

‡ Present address: Department of Microbiology and Immunology, Indiana University School of Medicine, Indianapolis, Indiana 46202-5120, USA.

recognition by members of the Ets family because they involve both strictly conserved amino acids and bases in the consensus sequence recognized by these transcription factors (see Fig. 3*b*). The equivalent arginines 81 and 84 in Ets-1 (ref. 9) do not contact the GGAA bases, but intermolecular nuclear Overhauser effects between these arginines and DNA were observed in the Fli-1 NMR studies[7]. Lys 245 extends from β3 just adjacent to the loop ('wing'), and Lys 219 is located in the 'loop' of the HTH motif. Lys 245 contacts the phosphate backbone of the GGAA strand in the minor groove upstream from the core sequence (Fig. 3*c*) and Lys 219 forms a salt bridge with the phosphate backbone of the opposite strand downstream of the GGAA core (Fig. 3*d*). Substitutions of glycine at each of these four conserved sites abolished DNA binding, confirming the functional importance of these contacts (see Fig. 2).

Mutations of conserved residues that contact the phosphate backbone also affect DNA binding. Substitution of glycine at Leu 174 or Trp 215 abolished DNA binding in PU.1. Similarly, substitution of any amino acid in Ets-1 (ref. 14) at the equivalent of PU.1 residues Lys 219 and Arg 222 that bind the phosphate backbone disrupted DNA binding. These minor-groove contacts might represent a conserved pattern for protein 'docking' in the Ets family. In Fli-1 (ref. 7), the equivalents of Leu 174, Lys 219 and Lys 222 showed large chemical shifts on DNA binding in the NMR studies (the counterpart of Trp 215 was buried).

Water molecules also participate in protein–DNA recognition in the PU.1 complex (Fig. 2). There are 27 well-ordered solvent molecules around the DNA. Solvent molecules in the major groove are hydrogen-bonded to the bases and also form a hydrogen-bonded network between the two strands that might contribute to the stability of the duplex and consequently influence specific DNA recognition. Conserved Arg 232 and Arg 235 each form direct and water-mediated contacts with the bases. Three other residues also contact DNA bases through water molecules: Thr 226, Gln 228 and Asn 236. These residues are not conserved in the Ets family and might represent interactions that are unique to the PU.1 protein. Thr 226 and Gln 228, at the amino-terminal end of helix α3, make water-mediated contacts with bases C25 and C26 respectively that are base-paired to guanines 8 and 9 in the core sequence.

TABLE 1 Structure determination and refinement

	Native	Hg	*I* (29)	*I* (13)	*I* (31)
Phasing statistics					
Resolution (Å)	2.3	3.0	2.9	3.0	2.8
Observed reflections	60,095	25,081	20,709	20,512	23,308
Unique reflections	20,105	14,902	13,258	12,910	15,397
Completeness (%)	97	79	65	69	68
R_{sym} (%)*	5.0	3.6	4.0	4.3	3.6
R_{iso} (%) to 3.0 Å†		13.0	14.4	15.9	13.0
Number of sites		2	2	2	2
For isomorphous data ($I/\sigma \geqslant 3$)					
Phasing power‡		1.33	1.76	1.04	0.98
To resolution (Å)		3.0	3.0	3.0	3.0
R_{Cullis}§		0.62	0.57	0.68	0.67
For anomalous data ($I/\sigma \geqslant 3$)					
Phasing power		1.0	1.41	1.13	1.43
To resolution (Å)		3.0	3.0	3.0	3.0
Mean figure of merit (10–3.0 Å) is 0.65.					
Refinement statistics					
Resolution range		8–2.3 Å			
Average *B* (Å^2)		20.1			
Crystallographic *R*-factor (%)		23.7			
R_{free} (%)[16]		29.9			
Number of reflections used		16,898 $F > 3\sigma(F)$			
Number of protein atoms		1,486			
Number of DNA atoms		1,300			
Number of solvent atoms		88			

The crystallization of the PU.1 ETS domain (residues 160–272) with a 16-bp synthetic DNA oligonucleotide containing the recognition sequence was described previously[6]. Crystals formed in the space group C_2 with $a = 89.1$, $b = 101.9$, $c = 55.6$ Å and $\beta = 111.2°$, with two complexes in the asymmetric unit. **Phase determination**. Four heavy-atom derivatives were prepared by soaking crystals of the native complex and by co-crystallizing iodinated oligonucleotides with the PU.1 domain. The locations of the iodinated bases are indicated in Fig. 2. Multiple isomorphous replacement phases, including anomalous data, were calculated. The package PHASES[17] was used to refine heavy-atom positions, *B*-factor/occupancies and to calculate phases to 3.0-Å resolution with an overall figure of merit of 0.65. The initial MIRAS map (3.0 Å) was improved by solvent flattening by the method of Wang[18] and with non-crystallographic density averaging. **Model building and refinement**. The improved MIRAS electron-density map was used to build the model with the interactive graphics programs TOM based on FRODO[19] and O[20]. The density for the DNA helix was a prominent feature of the map. To fit the DNA, an 'ideal' B–DNA duplex was generated with the program QUANTA (Molecular Simulations, Inc.) and fitted to the density as a rigid body. After the DNA was positioned, a polyalanine chain was constructed with the BONES option of the Alberta/Caltech program TOM. Subsequently side chains for all residues with clear electron density were added to the model. There were 11 disordered residues at the N terminus of the domain and 14 disordered residues at the C terminus so these amino acids were not included in the model. For all other residues representing the complete ETS domain, the electron density was clear (see Fig. 1) and allowed unambiguous fitting of both backbone and side-chain atoms. Manual adjustments of individual DNA bases were made to fit the electron density. In the program X-PLOR[21], the stereochemistry of the protein was optimized to bond and angle parameters developed by Engh and Huber[22] and for DNA by using parameters of Parkinson *et al.*[23]. Weak restraints were placed on all ribose conformations. One cycle of simulated annealing at 3,000 K (ref. 24) was followed by cycles of manual model building, positional refinement and *B*-factor refinement. More data were added as the refinement progressed in increments: 3, 2.8, 2.6 and 2.3 Å. A total of 88 solvent oxygens ($\langle B \rangle = 22$ Å^2) have been added to the model at this stage of the refinement. Main-chain torsion angles for all non-glycine residues fall within energetically favourable Ramachandran boundaries[25]. The r.m.s. difference for 84 α-carbon atoms in the two complexes in the asymmetric unit is 0.35 Å.

* R_{sym} is $\sum |I - \langle I \rangle| / \sum \langle I \rangle$.

† R_{iso} is $\sum ||F_{PH}| - |F_P|| / \sum |F_P|$, where $|F_P|$ and $|F_{PH}|$ are structure factors for the protein and derivative, respectively.

‡ Phasing power is the r.m.s. value of $|F_H|/E$, where E is residual lack of closure.

§ $R_{Cullis} = \sum ||F_{PH}| \pm |F_P| - |F_{H(calc)}|| / \sum |F_{PH} - F_P|$ for centric reflections, where $F_{H(calc)}$ is the calculated heavy-atom structure factor.

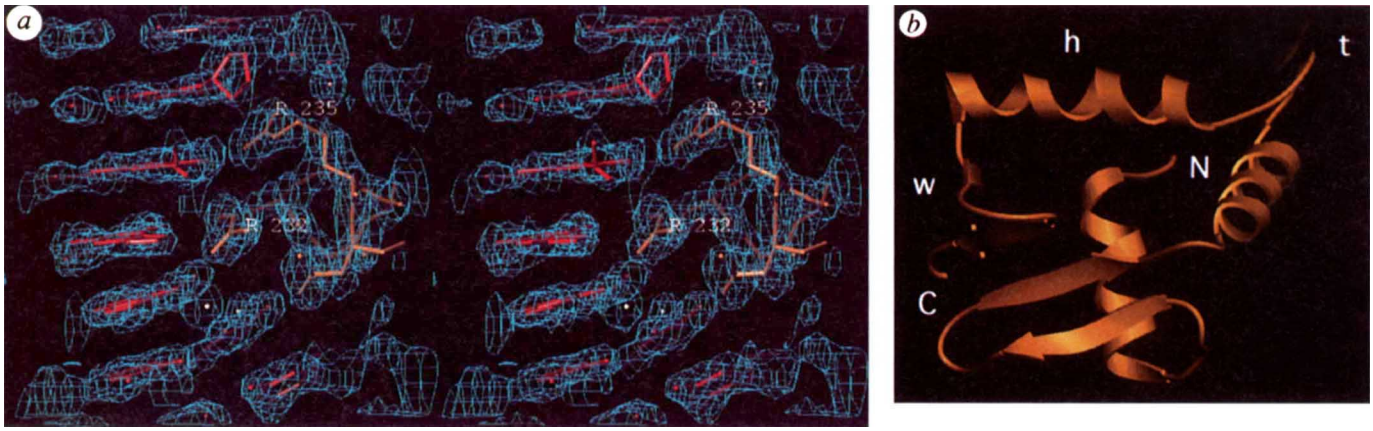

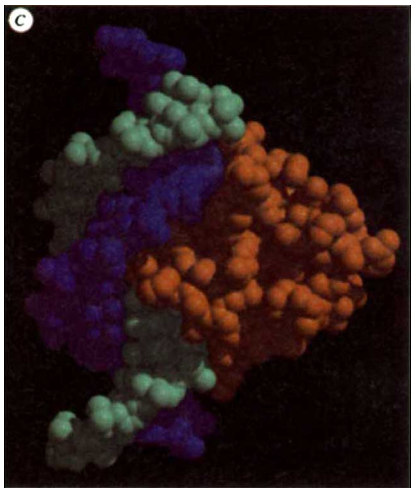

FIG. 1 Overall structure of the PU.1–DNA complex. *a*, Stereoview of the refined 2.3-Å (1.5 σ) $2|F_o| - |F_c|$ electron-density map at the protein–DNA interface. Interactions of protein (gold), DNA (red) and water (white) in the major groove at the GGAA core recognition sequence are shown. The two strictly conserved residues, Arg 232 and Arg 235 from recognition helix α3, make direct contact with bases in the major groove. There is a tight network of water molecules at this site in the major groove (Fig. 2). *b*, Ribbon drawing of the PU.1 ETS domain. The module (residues 171–258) is composed of three α-helices and a four-stranded antiparallel β-sheet. In the interior of the domain, a hydrophobic core is formed with 19 side chains including seven strictly and eight highly conserved residues. The major structural features that contact the DNA are indicated: the recognition helix α3 (h), the turn in the HTH motif (t) and the loop between β-strands 3 and 4 (w) corresponding to the 'wing' in these proteins. At the N-terminal end of the fragment, helix α1 begins at residue 172. The C-terminal segment, which is disordered in the PU.1–DNA complex, assumes an α-helical conformation in the unbound Ets-1 NMR structure[8]. This segment might unfold in PU.1 with DNA binding. *c*, Space-filling model of the PU.1 ETS domain–DNA complex. Protein–DNA interactions include both major and minor groove contacts over a distance of 30 Å. The PU.1 transcription factor (gold) binds to DNA as a monomer, so it is not surprising that extensive DNA contact sites exist in addition to the recognition sequence to stabilize binding. HNF-3γ (ref. 12) and GH5 (ref. 11) also bind to target DNA as monomers. In the HNF-3γ–DNA complex, three regions were involved in DNA recognition: the recognition helix and two 'wings'. The location of the first 'wing' between the last two strands in the β-sheet corresponds topologically to the 'wing' in PU.1, but contacts from the second 'wing' emanate from a loop at the C terminus of the domain. The structural equivalent to the second 'wing' is absent in PU.1.

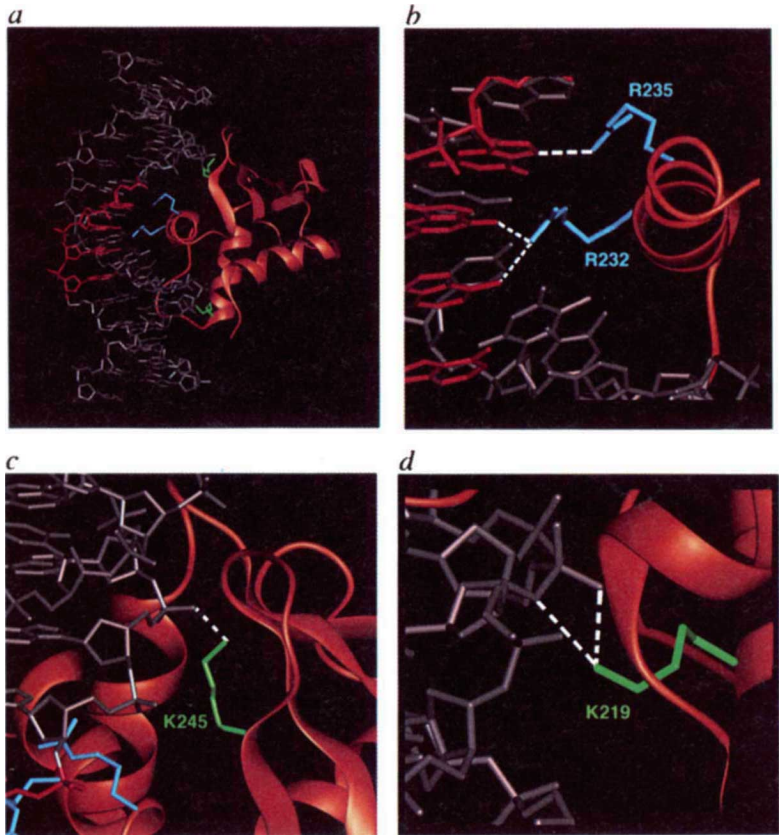

FIG. 3 PU.1–DNA complex. *a*, The 16-bp oligonucleotide bound in complex to the PU.1 ETS domain is shown in grey, with the GGAA sequence coloured red. The ETS domain is represented by an orange ribbon model with the side chains for four conserved residues that contact DNA shown. When glycine was introduced at each of these sites, DNA binding was lost (Fig. 2). *b*, Detailed close-up view, showing that Arg 232 and Arg 235 from the recognition helix make hydrogen bonds with the bases GGA of the PU core sequence. Arg 235(NH2) forms a hydrogen bond with G8(O6), whereas Arg 232(NH1) makes hydrogen bonds with two bases G9(O6) and A10(N6). These arginines are strictly conserved in all members of the Ets family, and the GGA sequence is the consensus DNA sequence recognized by the Ets proteins. Therefore the interactions shown here represent the paradigm for Ets recognition, which is expected to be reproduced in all Ets protein–DNA complexes. *c*, Interaction of the 'wing': Lys 245(NZ) contacts the phosphate backbone at G6(O2P). *d*, Interaction of Lys 219(NZ) from the loop in the HTH motif, which contacts the phosphate backbone at C22(O3P) and T23(O2P). This figure was generated with the graphics program QUANTA (Molecular Simulations, Inc.).

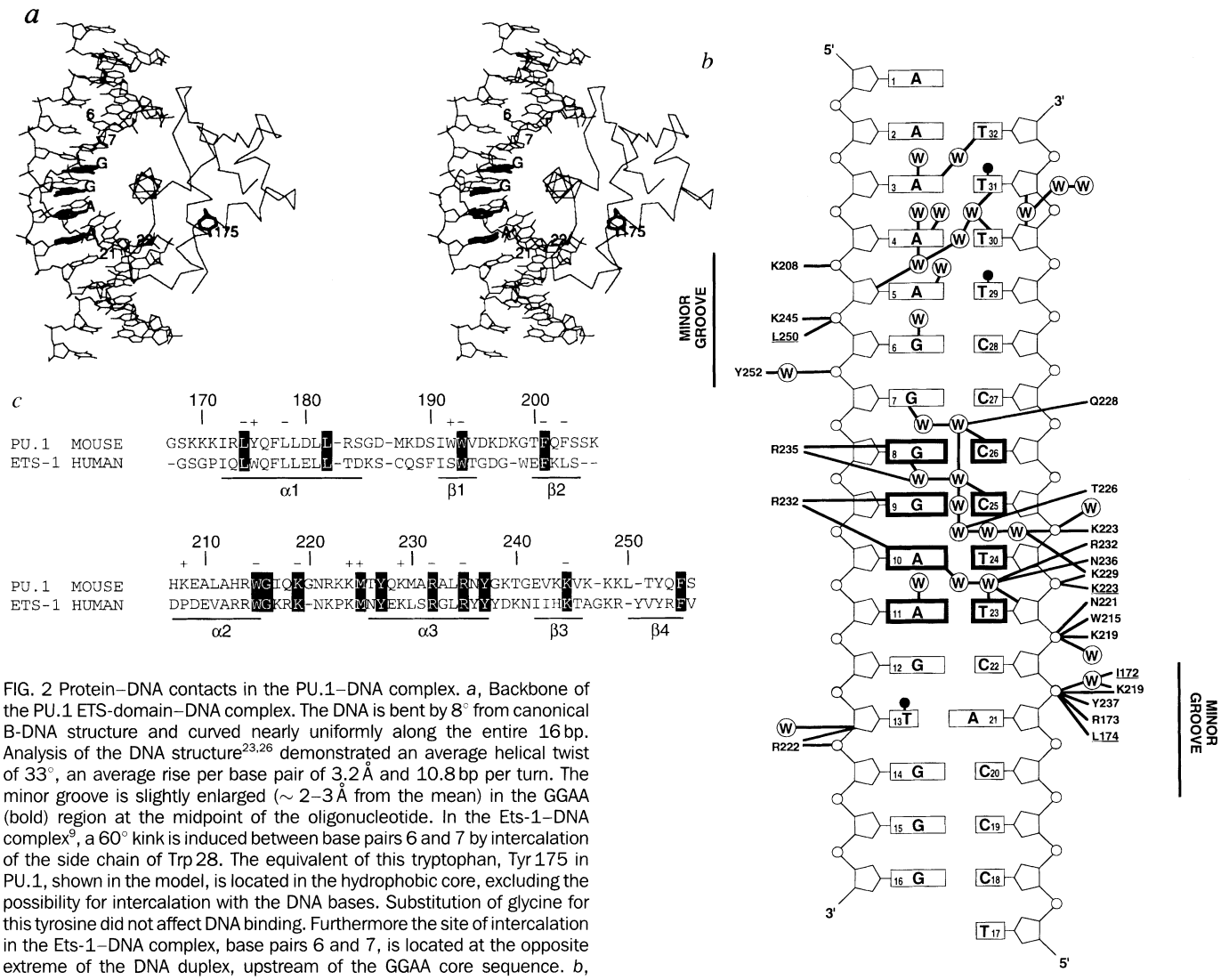

FIG. 2 Protein–DNA contacts in the PU.1–DNA complex. *a*, Backbone of the PU.1 ETS-domain–DNA complex. The DNA is bent by 8° from canonical B-DNA structure and curved nearly uniformly along the entire 16 bp. Analysis of the DNA structure[23,26] demonstrated an average helical twist of 33°, an average rise per base pair of 3.2 Å and 10.8 bp per turn. The minor groove is slightly enlarged (~ 2–3 Å from the mean) in the GGAA (bold) region at the midpoint of the oligonucleotide. In the Ets-1–DNA complex[9], a 60° kink is induced between base pairs 6 and 7 by intercalation of the side chain of Trp 28. The equivalent of this tryptophan, Tyr 175 in PU.1, shown in the model, is located in the hydrophobic core, excluding the possibility for intercalation with the DNA bases. Substitution of glycine for this tyrosine did not affect DNA binding. Furthermore the site of intercalation in the Ets-1–DNA complex, base pairs 6 and 7, is located at the opposite extreme of the DNA duplex, upstream of the GGAA core sequence. *b*, Sequence of the oligonucleotide bound to the PU.1 protein (GGAA PU box in bold lines). Residues that contact the DNA through main-chain atoms are underlined. Well-defined solvent molecules located within 3.2 Å of protein or DNA atoms are identified by an encircled W. Contacts from residues of the 'wing' are made with the nucleotides upstream of the GGAA sequence, and residues from the loop in the HTH motif interact with the opposite strand, downstream of the GGAA site. The direction of the DNA was confirmed by the location of the three iodinated bases (13,29,31; black dots) used for phase calculation. Seven of the residues that contact DNA are strictly conserved and four others are highly conserved. *c*, Sequence alignment of the PU.1 and Ets-1 ETS domains, representing extremes of evolutionary divergence in the family. Residues strictly conserved in all Ets proteins are shown in black boxes; dashes indicate gaps within the family. Numbering and secondary structural features of the PU.1 domain are indicated. The results of mutational analysis when glycine was substituted for a residue are also shown. The effects of the interchanges are labelled + or – above the sequence, indicating that DNA binding was retained or abolished. Mutations were generated essentially as described[27].

The turn in the HTH motif is actually a loop, and because the sequences in this loop as well as the loop ('wing') between strands β3 and β4 are not strictly conserved among members of the Ets family, these residues might be important sites for specific recognition by individual members of the family. In fact, the lengths of both of the contact loops differ among members of the family, with the PU.1 loop containing an 'extra' glycine at residue 220 and lacking a glycine after residue 247. Such conformational differences are expected between family members, but the contrast between the PU.1 and Ets-1 complexes was unexpected. The striking distinction in the mode of DNA contact by the PU.1 and Ets-1 domain could reflect extreme evolutionary divergence between members of the Ets family. Alternatively, it should be noted that the Ets-1–DNA complex was formed under denaturing conditions[9,15] and it is possible that the Trp intercalation occurred early during the renaturation step with subsequent protein refolding.

Future extensive mutational studies of amino acids that contact DNA in Ets proteins are needed to identify residues that mediate recognition of a specific DNA sequence by a given family member. Ultimately, crystal structures of other Ets proteins complexed to DNA must be compared to distinguish unique DNA contacts. □

Received 12 January; accepted 19 February 1996.

1. Wasylyk, B., Hahn, S. L. & Glovane, A. *Eur. J. Biochem.* **211,** 7–18 (1993).
2. Moreau-Gachelin, F. *Biochim. biophys. Acta* **1198,** 149–163 (1994).
3. Karim, F. *et al. Genes Dev.* **4,** 1451–1453 (1990).
4. Klemsz, M. J., McKercher, S. R., Celada, A., Van Beveren, C. & Maki, R. A. *Cell* **61,** 113–124 (1990).
5. Moreau-Gachelin, F., Mattei, M. G., Tambourin, R. & Tavitian, A. *Oncogene* **4,** 1449–1456 (1989).
6. Pio, F. *et al. J. biol. Chem.* **270,** 24258–24263 (1995).
7. Liang, H. *et al. Nature struct. Biol.* **1,** 871–875 (1994).
8. Donaldson, L. W., Petersen, J. M., Graves, B. J. & McIntosh, L. P. *EMBO J.* **15,** 125–134 (1996).
9. Werner, M. H. *et al. Cell* **83,** 761–771 (1995).
10. Schultz, S. C., Shields, G. C. & Steitz, T. A. *Science* **253,** 1001–1007 (1991).

11. Ramakrishnan, V., Finch, J. T., Graziano, V., Lee, P. L. & Sweet, R. M. *Nature* **362,** 219–223 (1993).
12. Clark, K. L., Halay, E. D., Lai, E. & Burley, S. K. *Nature* **364,** 412–420 (1993).
13. Harrison, C. J., Bohm, A. A. & Nelson, H. C. M. *Science* **263,** 224–227 (1994).
14. Mavrothalassitis, G., Fisher, R. J., Smyth, F., Watson, D. K. & Papas, T. S. *Oncogene* **9,** 425–435 (1994).
15. Werner, M. H., Clore, G. M., Gronenborn, A. M., Kondoh, A. & Fisher, R. J. *FEBS Lett.* **345,** 125–130 (1994).
16. Brünger, A. T. *Nature* **355,** 472–475 (1992).
17. Furey, W. & Swaminathan, S. *Am. crystallogr. Ass. Meeting* **18,** 73 (1990).
18. Wang, B. C. *Methods Enzymol.* **115,** 90–112 (1985).
19. Jones, T. A. *Methods Enzymol.* **115,** 157–171 (1985).
20. Jones, T. A., Zhou, J., Cowan, S. W. & Kjeldgaard, M. *Acta crystallogr.* **A47,** 110–119 (1992).
21. Brünger, A. T. *X-PLOR Manual* Version 3.1 (Yale Univ. Press, New Haven, CT, 1992).
22. Engh, R. A. & Huber, R. *Acta crystallogr.* **A57,** 392–400 (1991).
23. Parkinson, G., Vojtechovsky, J., Clowney, L., Brünger, A. T. & Berman, H. M. *Acta crystallogr.* **D52,** 57–64 (1996).
24. Brünger, A. T., Krokowski, A. & Erickson, J. W. *Acta crystallogr.* **A46,** 585–593 (1990).
25. Ramachandran, G. N. & Sasiekharan, V. *Adv. Protein Chem.* **23,** 283–438 (1968).
26. Babcock, M. S. & Olson, W. K. *J. molec. Biol.* **237,** 98–124 (1994).
27. Ho, S. N., Hunt, H. D., Horton, R. M., Pullen, J. K. & Pease, L. R. *Gene* **77,** 51–59 (1989).

ACKNOWLEDGEMENTS. This work was supported by grants from the U.S. Army and NIH. R.K. and F.P. made equal contributions to this study. We thank J. Knight and R. Mitchell for synthesis and purification of DNA oligonucleotides, M. Hasham for excellent graphics illustrations, and K. Riddle-Hilde for preparing the manuscript for publication.

CORRESPONDENCE AND MATERIALS. Requests to be addressed to K.R.E.

CORRECTION

Rapid energy dissipation and variability of the Io–Jupiter electrodynamic circuit

Renée Prangé, Daniel Rego, David Southwood, Philippe Zarka, Steven Miller & Wing Ip

Nature **379,** 323–325 (1995)

In Fig. 1 of this Letter, a dashed line was omitted that was referred to in the legend to Fig. 3*a*. The corrected figure is shown here.

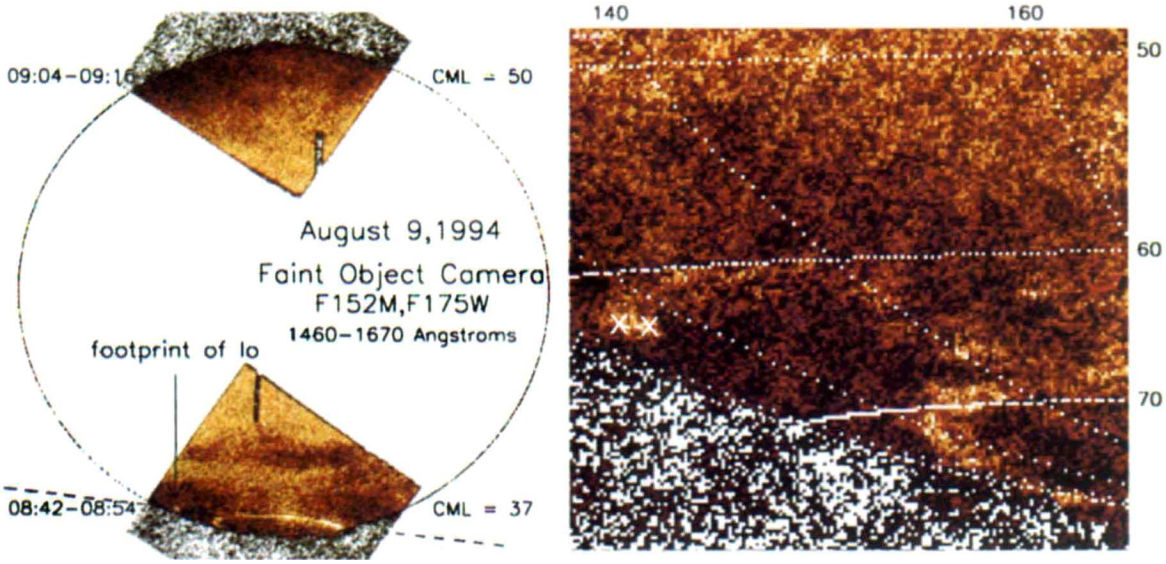

Images of the FUV Jovian aurorae and of the far-ultraviolet signature of the Io magnetic flux tube with the Hubble Space Telescope Faint Object Camera (*f*/96). The plot in Fig. 3*a* was taken along the dashed line in the left image, across the south Io footprint and the auroral oval.